ARTICLE NO. 77-1166

High-Fidelity Airplane Simulation Model

Hozo Yoshino*
Boeing Commercial Airplane Company, Seattle, Wash.

A separate wing-body and tail simulation model has been developed for real-time digital computer application. This model has displayed a potential capability in reproducing the real airplane's dynamics faithfully. The model derives the aerodynamic forces and moments of the airplane's wing-body and tail separately, which are then combined at the airplane's center of gravity. The mechanization provides insight into the relative contributions of these components to the airplane's balance and dynamics. It permits unsteady aerodynamic effects to be accounted for at local aerodynamic surfaces. The formulation has become possible after defining a local kinematic angle-of-attack rate using the airplane's geometrical dimensions and associated kinematic variables. Real-world physics such as wing wake/downwash, engine exhaust, wind/gust, ground effects, and structural elasticity may be readily accommodated into the model, and more accurate formulation of dynamic derivatives of aerodynamic surfaces can be defined. The mechanization offers the possibility of more efficient computer utilization with multicalculation rates. A fixed base piloted simulation was conducted. Some preliminary results of computer simulation are presented.

Introduction

MOST airplane simulation models employ a complete wing-body-tail combination. References 1-3 are well-utilized textbooks of aircraft stability and control simulation science and their equations are based on the small-perturbation method mechanized for a combined wing-body-tail configuration. Although this formulation has the advantage of lending itself to simple computer simulations for basic airplane stability and performance analysis, it is not suited for the simulations of a large airplane maneuver. In this regard, industry and research organizations presently use the more general equations which allow the inclusion of some nonlinear effects. References 4 and 5 summarize the equations of motion applicable to large airplane maneuvers with their formulations made for the combined wing-body-tail configurations. The present Boeing simulation models[6,7] are based on the equations of motion given in Ref. 4. This approach still has some shortcomings in reproducing airplane's forced transient responses faithfully.

This fact has led Boeing to develop a separate wing-body and tail simulation model. A longitudinal three-degree-of-freedom simulation model was developed for the Boeing 707 engineering simulator as a test case for its capability. This paper summarizes the approach made and the results obtained for this study. The Boeing 767/777 and 757 programs are currently developing six-degree-of-freedom separate wing-body and tail simulation models.

Figure 1 shows the schematic of the formulation of the separate wing-body and tail simulation model. As this model uses local aerodynamic arguments (airspeed, angle of attack, etc.) for the wing-body and tail, the corresponding aerodynamic data base from wind-tunnel testing is directly utilized.

This formulation provides better insight into the contributions of the wing and tail to the airplane's balance and dynamics. Since it permits unsteady aerodynamic effects to be accounted for at local aerodynamic surfaces, wing and tail airload time histories and their mutual interferences can be visualized. This approach is therefore well suited for airplane configuration development where the wing and tail are varying during the airplane optimization process. The separate wing-body and tail data base in the simulator can be readily adjusted for size and location. This separate wing-body and tail model was formulated on a real-time digital computer, the EAI 8400. Computational sequencing and cycle time required careful consideration on the digital machine for which each subsystem was modularized and allocated its own frame time according to its natural frequency.

Presented as Paper 77-1166 at the AIAA Atmospheric Flight Mechanics Conference, Hollywood, Fla., Aug. 8-10, 1977; submitted Sept. 12, 1977; revision received Sept. 11, 1978.

Index categories: Handling Qualities, Stability and Control; Simulation; Nonsteady Aerodynamics.

*Senior Engineer, Flight Controls Technology. Member AIAA.

Simulator Mechanization

Longitudinal Control System

As this was a real-time man-machine system, care was taken to simulate the control systems adequately. The flow diagram of the Boeing 707 longitudinal control system is shown in Fig. 2. The pilot exerts a force F_S on the control column, rotating it to produce the control column angle δ_C. This angular deflection is transmitted to the aft-quadrant through the control cables, causing the aft-quadrant to rotate giving the aft-quadrant angle δ_{AQ}. This angular deflection causes the elevator control tab and in turn the elevator to rotate, generating the control tab angle δ_{ET} and elevator angle δ_E, respectively. The stabilizer actuated elevator tab (*SAET*) angle δ_{SAET} is controlled by the cam program, being a function of the elevator angle and stabilizer angle δ_{FRL}, the latter is set by the stabilizer trim actuator. Since this longitudinal control system is manually operated, the control surface dynamics are fed back to the pilot as a control column feel force.

In setting up the dynamic equations of the longitudinal control system, each subsystem in the system was assumed to be subject to aerodynamic, field-induced (i.e., gravity and inertia force), and mechanical hinge moments. Aerodynamic hinge moment data were obtained from full-scale NASA 40×80-ft wind-tunnel test on the Boeing 720B horizontal tail.[8] Equations for both field-induced and mechanical moments were developed using production drawings.

Each subsystem had a different time constant. For a subsystem which related to the rigid airplane motion, a frame time of about 40 ms was assigned. Subsystems which had medium time constants of 100 to 300 ms such as the control column and elevator, were assiged a 10-ms frame time. For the subsystems which had the smallest time constants, such as the aft-quadrant and control tab, the iteration frame time was 2.5 ms. As the time constants were very small for the latter

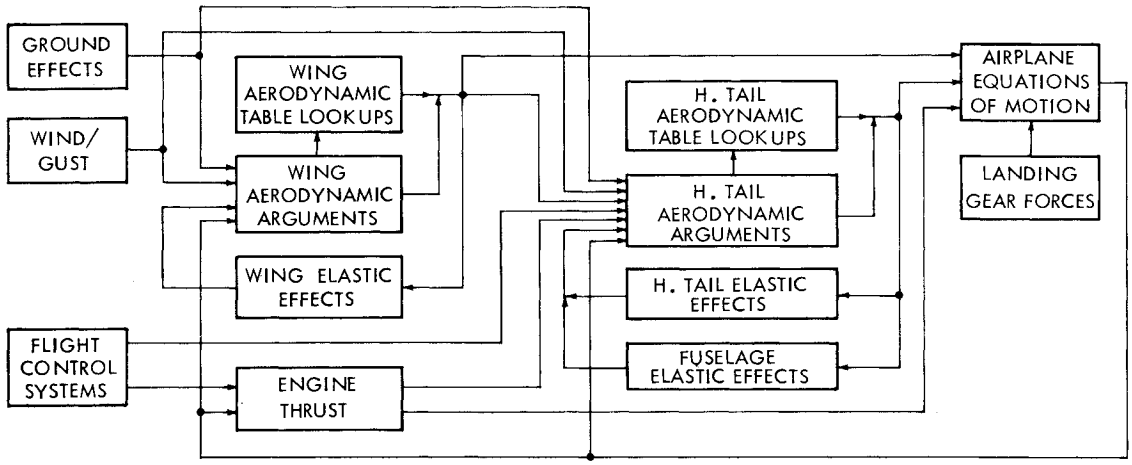

Fig. 1 Formulation of the separate wing-body and tail simulation model.

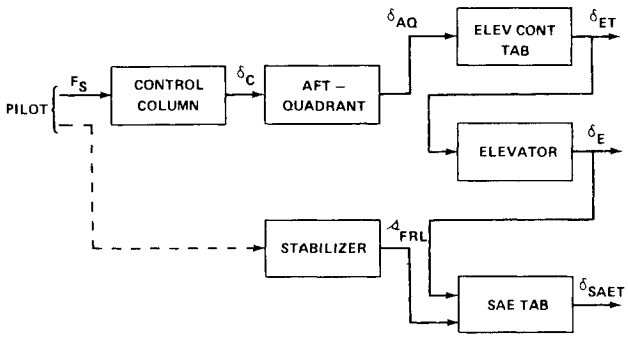

Fig. 2 Flow diagram of 707 longitudinal control system.

subsystems, the damping ratios were arbitrarily increased to be compatible with the frame time. Experience had shown that about 100 ms corresponded to the fastest time constant that a human pilot could distinguish.

The multicalculation rates selected for this study minimized computer cycle time to about 40 ms without compromising pilot handling qualities.

Definition of Kinematic Angle of Attack

As shown in Fig. 3, the wing and tail angles of attack and time rates due to airplane kinematics were defined separately using the airplane's variables at its center of gravity and the moment arms to the local aerodynamic reference points. This definition transformed the kinematic variables into local aerodynamic arguments, which were input into the aerodynamic data base.

Whenever a local point is displaced from the airplane's center of gravity, its translational acceleration due to the rotational acceleration of the airplane is additive to that of the airplane's center of gravity as indicated in Fig. 3. The magnitude and phase relationship of this modulation is a function of the rotational acceleration and moment arm. For the derivation of local kinematic angle of attack and time rate, see the Appendix.

Wing Wake, Downwash, and Engine Exhaust

Wing wake, wing downwash, and engine exhaust modify the horizontal tail aerodynamic arguments. These effects were combined with the kinematically defined arguments discussed earlier. The wing wake coefficient K_W was defined as the ratio of the airspeed loss by wake, ΔV_{WB}, to the wing-body reference airspeed V_{WB} and based on data from the existing simulator document[7]:

$$\Delta V_{WB} = K_W V_{WB}$$

Wing downwash ΔW_{WB} was assumed to be proportional to the wing circulation Γ_W which is, in turn, proportional to the wing-body lift coefficient C_{LWB} multiplied by the wing-body reference airspeed V_{WB} divided by the wing aspect ratio $\mathcal{R}$.[1]

$$\Delta W_{WB} = \frac{2K_E}{\pi \mathcal{R}} C_{LWB} V_{WB} \propto \Gamma_W$$

The proportionality coefficient K_E was determined from the wind-tunnel test results and is equal to 0.966.[9] To be compatible with the definition of kinematic angle of attack, derivative forms of these effects were developed. The transportation lag $e^{-\tau s}$ was accommodated in the digital computer as $e^{-m\Delta tz}$, where Δt is computer cycle time and m is an integer closest to simulate τ. τ is the time needed for the airmass to travel from the wing mean aerodynamic quarter chord line to the horizontal tail reference line. The effect of the wing wake at the horizontal tail K_{WW} was modeled using a Gaussian weighting factor, defined as a function of the tail fuselage angle of attack α_{TFRL}. The effect of the wing downwash at the horizontal tail K_{DW} was similarly modeled using K_{WW}. Figure 4 illustrates the wing-body induced airstream acceleration at the horizontal tail.

Equations of the airstream acceleration at the horizontal tail reference line due to these effects were converted into the body x and z axis components as follows:

$$\Delta \dot{u}_T = \cos\alpha_{WB} \cdot \Delta \dot{V}_{TW} - \sin\alpha_{WB} \cdot \Delta \dot{W}_{TW}, \text{ft/s}^2$$

$$\Delta \dot{w}_T = \sin\alpha_{WB} \cdot \Delta \dot{V}_{TW} + \cos\alpha_{WB} \cdot \Delta \dot{W}_{TW}, \text{ft/s}^2$$

where $\Delta \dot{V}_{TW}$ is wind acceleration at the horizontal tail, caused by the wing airspeed change and its wake effect, delayed, and weighted by a function of the tail fuselage angle of attack, defined in the stability x axis:

$$\Delta \dot{V}_{TW} = K_{WW} \cdot e^{-m\Delta tz} \cdot K_W \cdot \Delta \dot{V}_{WB}, \text{ft/s}^2$$

and $\Delta \dot{W}_{TW}$ is wind downward acceleration at the horizontal tail, caused by the wing lift and airspeed changes, delayed, and weighted by a function of the tail fuselage angle of attack, defined in the stability z axis:

$$\Delta \dot{W}_{TW} = K_{DW} \cdot e^{-m\Delta tz} \cdot \frac{2K_E}{\pi \mathcal{R}} \cdot \frac{\mathrm{d}(C_{LWB} V_{WB})}{\mathrm{d}t} \text{ ft/s}^2$$

As the Boeing 707 is a manually powered airplane, the stick to elevator response is affected by dynamics of the airstream at the horizontal tail. By adjusting the wing wake and wing downwash effects, the longitudinal control response match

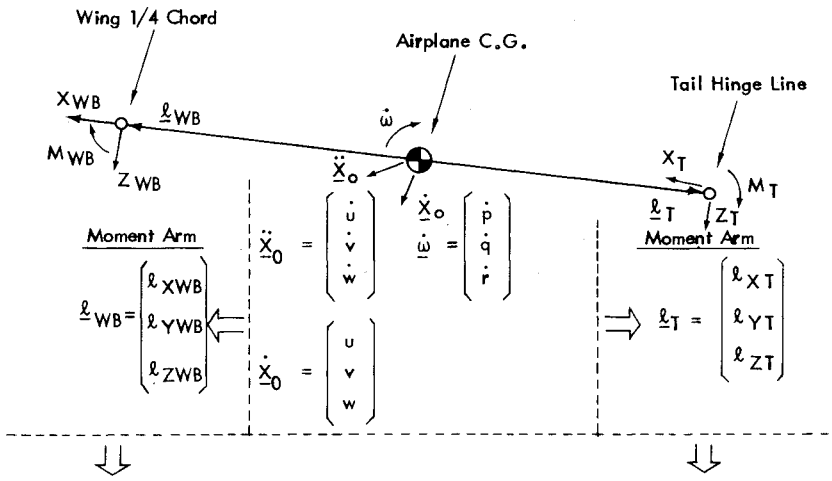

Fig. 3 Wing and tail kinematic angle of attack.

$$\dot{\alpha}_{WB} = \frac{180}{\pi}\,\frac{u_{WB}\dot{w}_{WB} - \dot{u}_{WB}w_{WB}}{u_{WB}^2 + w_{WB}^2}\ \text{deg/sec} \qquad \dot{\alpha}_T = \frac{180}{\pi}\,\frac{u_T\dot{w}_T - \dot{u}_T w_T}{u_T^2 + w_T^2}\ \text{deg/sec}$$

$$\alpha_{WB} = \int_o^t \dot{\alpha}_{WB}\,dt + \alpha_{WBO}\ \text{degrees} \qquad \alpha_T = \int_o^t \dot{\alpha}_T\,dt + \alpha_{TO}\ \text{degrees}$$

$$\dot{u}_{WB} = \dot{u} + \ell_{ZWB}\,\dot{q}\ \text{ft/sec}^2 \qquad \dot{u}_T = \dot{u} + \ell_{ZT}\,\dot{q}\ \text{ft/sec}^2$$

$$\dot{w}_{WB} = \dot{w} - \ell_{XWB}\,\dot{q}\ \text{ft/sec}^2 \qquad \dot{w}_T = \dot{w} - \ell_{XT}\,\dot{q}\ \text{ft/sec}^2$$

$$u_{WB} = \int_o^t \dot{u}_{WB}\,dt + u_{WBO}\ \text{ft/sec} \qquad u_T = \int_o^t \dot{u}_T\,dt + u_{TO}\ \text{ft/sec}$$

$$w_{WB} = \int_o^t w_{WB}\,dt + w_{WBO}\ \text{ft/sec} \qquad w_T = \int_o^t \dot{w}_T\,dt + w_{TO}\ \text{ft/sec}$$

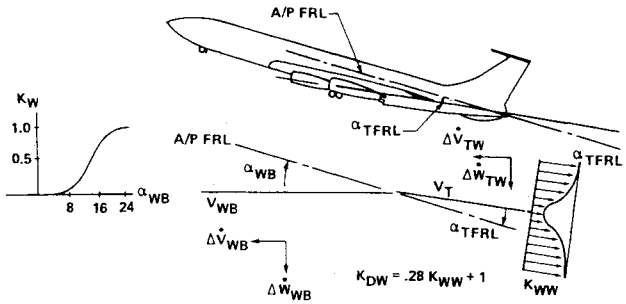

Fig. 4 Wing-body induced acceleration at the horizontal tail.

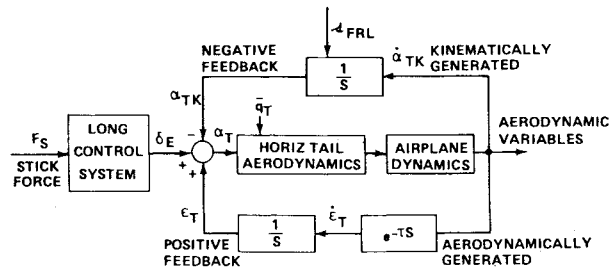

Fig. 5 Simulator formulation of the horizontal tail aerodynamic argument dynamics incorporating both kinematical and aerodynamic feedback effects.

was improved. Figure 5 illustrates the simulator formulation of the aerodynamic argument dynamics at the horizontal tail. Known physical characteristics of the manual control system were utilized to estimate the tail aerodynamic argument dynamics. Engine exhaust effects were similarly modeled.

Wind and Gust

Although wind and gust effects were not included in the present formulation, these effects can be readily accommodated into the model. The wing and tail can be treated separately for inclusion of wind and gust effects.

Ground Effects

Ground effects were also included as modifiers to the local aerodynamic arguments using the mirror image technique. To obtain the ground effects dynamic equations, the derivative form of Prandtl's equation describing the circulation on a lifting line was developed. By this formulation, the ground-induced airstream accelerations at the local points were defined as functions of the circulation rates and the ground effect correction factors (GEWB and GET) whose values were defined as functions of the ground heights (H_{WB} and H_T). Figure 6 shows how the ground effects were introduced into the wing-body aerodynamic argument equations. As noted in the previous paragraph on wing downwash, the wing-body circulation rate $d\Gamma_W/dt$ is described as

$$\frac{d\Gamma_W}{dt} \propto \frac{d(C_{LWB}V_{WB})}{dt} = C_{LWB}\frac{\partial V_{WB}}{\partial t} + \frac{\partial C_{LWB}}{\partial \alpha_{WB}}\frac{\partial \alpha_{WB}}{\partial t}V_{WB}$$

Wing-body ground effect correction factors GEWB1 and GEWB2 correct for the effects by the bound image vortices

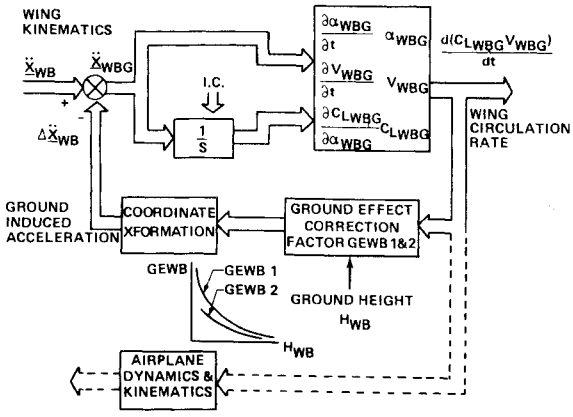

Fig. 6 Wing-body aerodynamic argument in ground effects.

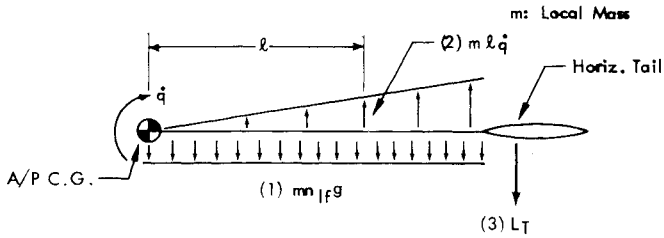

Fig. 7 Aft-fuselage bending due to various loadings.

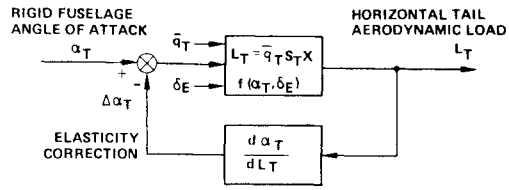

Fig. 8 Formulation of aft-fuselage bending due to tail airload.

and free image vortices, respectively, and are inversely proportional to the ground height squared. A similar derivation was made for the horizontal tail. Since downwash angle is also affected by the ground plane, the downwash correction factor (DWCF) was defined to modify the free air downwash angle. DWCF is a function of wing ground effect correction factor GEWB2.

Stuctural Elasticity Effects

The wing, tail, and fuselage were treated independently for inclusion of structural elasticity effects. Considered as inputs were normal load factor at the center of gravity and pitch angular acceleration, as well as the wing and horizontal tail airloads. As an example, consider the fuselage bending effects. Shown in Fig. 7 are three forces acting on the airplane aft-fuselage. These are 1) force acting on the airplane center of gravity as a function of normal load factor n_{lf}, 2) force generated by the rotational acceleration of the airplane $\dot{q}$, and 3) force acting on the horizontal tail L_T. By this formulation, a quasistatic fuselage bending mode was accommodated as a modifier to local aerodynamic arguments.

Figure 8 illustrates the effect of the horizontal tail airload L_T on the tail angle of attack α_T. This mechanization is a more efficient way to include elasticity effects compared to using a series of three-dimensional table lookups for aerodynamic stability coefficients corrections.

Dynamic Derivatives

To be compatible with the definition of the local angle-of-attack rate, new dynamic derivatives for aerodynamic surfaces were defined. The assumptions made for the calculation

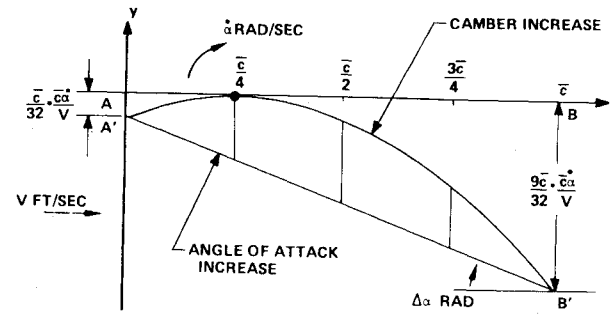

Fig. 9 Rotating airfoil seen by oncoming airflow.

are as follows:

1) Aerodynamic surfaces rotation about the reference line is at constant rate.
2) Airflow is assumed to adjust itself to the angle-of-attack change instantaneously.
3) Control surfaces are not deflected.
4) Spanwise aerodynamic loading is proportional to the local chord length.
5) No structural deflections.
6) No air compressibility effect.

At low speed and moderate angle of attack in a steady-state condition, the pressure distribution on an aerodynamic surface is solely determined by its relative translational motion with respect to the airstream once the shape of the aerodynamic surface is given. The relative motion, however, will be modulated by the rotational motion of the aerodynamic surface. An observer attached to the oncoming airflow with the velocity V will see the airfoil camber line rotated and bulged from the original horizontal position AB as shown in Fig. 9 when the mean aerodynamic chord rotates about its quarter chord line at $\dot{\alpha}$ rad/s.

In view of the spanwise behavior, a local aerodynamic chord displaced from the mean aerodynamic chord will experience additional angle-of-attack change because of the relative moment arm due to surface sweep angle and rotational velocity. The effective angle-of-attack and camber changes will produce the incremental change in aerodynamics or dynamic derivatives.

A two-dimensional potential flow computer program with a 10-strip half-wing approximation was used along with wind-tunnel test results to calculate the wing and horizontal tail dynamic derivatives. Table 1 summarizes the equations of dynamic derivatives for the separate wing-body and tail simulation model. Angle-of-attack rates used were non-dimensionalized by local aerodynamic mean chords and airspeeds, $c_L/2V_L$, and the dynamic derivatives were defined in rad/airtime.

The dynamic derivatives calculated represent the values at low unsteady aerodynamic frequencies associated with rigid airplane modes. The present combined wing-body-tail

Table 1 Equations for dynamic derivatives[a]

Wing	Horizontal tail
$C_{LW}\hat{\alpha}_{WB} = 40.8\dfrac{\partial C_{LWB}}{\partial \alpha_{WB}}$	$C_{LT}\hat{\alpha}_T = 38.5\dfrac{\partial C_{LT}}{\partial \alpha_T}$
$C_{DW}\hat{\alpha}_{WB} = 2.76\,C_{LWB}\dfrac{\partial C_{LWB}}{\partial \alpha_{WB}}$	$C_{DT}\hat{\alpha}_T = 22.8\dfrac{\partial C_{DT}}{\partial \alpha_T}$
$C_{MW}\hat{\alpha}_{WB} = -40.7\dfrac{\partial C_{LWB}}{\partial \alpha_{WB}}$	$C_{MT}\hat{\alpha}_T = 28.7\dfrac{\partial C_{MT}}{\partial \alpha_T} - 9.6\dfrac{\partial C_{LT}}{\partial \alpha_T}$

[a] Lift, drag, and pitching moment curve slopes are defined in deg^{-1}

simulation model has much larger dynamic derivatives[7] relative to those of the estimation made for the separate wing-body and tail model. This could be attributed to the phase lead nature of the $\dot{\alpha}_T$ derivatives in the separate wing-body and tail model due to the contribution from the $\dot{q}$ term, as the tail surface experiences the angle-of-attack change at the same time the airplane feels the pitching moment imbalance.

Aerodynamic Data

NASA 40×80-ft wind-tunnel test data on the Boeing 720B horizontal tail[8] were used to extract the tail aerodynamic characteristics. This test result indicated that the present combined wing-body-tail model has higher stabilizer and elevator effectivenesses on the pitching moment compared to those of the estimation made for the separate wing-body and tail model.

Wing-body aerodynamic characteristics were obtained from the University of Washington low-speed wind-tunnel test on a Boeing 707-320B(ADV)/C model.[9] Flight test results were applied to include scale effects. These separate wing-body and tail aerodynamic data were stored in the computer mostly as two-dimensional table lookups.

Mach Effects

Mach effects were not included in the present simulation model. However, they can be efficiently accommodated into the separate wing-body and tail data base. Mach effects including Glauert-Prandtl compressibility corrections can be applied separately to the wing-body and tail aerodynamic arguments rather than having a series of three-dimensional table lookups for aerodynamic stability coefficients corrections.

Longitudinal Aerodynamic Equations

Aerodynamic stability coefficients were defined at the wing mean aerodynamic quarter chord line and horizontal tail reference line, as functions of the respective aerodynamic arguments defined at the local points. The aerodynamic stability coefficients were then dimensionalized using the reference dimensions and local dynamic pressures. These dimensionalized forces and moments were combined at the airplane's center of gravity. These equations are presented in the following (see Fig. 3 for nomenclature definition):

X-Direction Force (X_{AERO})

$$X_{AERO} = X_{WB} + X_T, \text{ lb}$$

Z-Direction Force (Z_{AERO})

$$Z_{AERO} = Z_{WB} + Z_T, \text{ lb}$$

Moment about Y Axis through c.g. (M_{AERO})

$$M_{AERO} = M_{WB} + l_{ZWB} \cdot X_{WB} - l_{XWB} \cdot Z_{WB} + M_T + l_{ZT} \cdot X_T - l_{XT} \cdot Z_T, \text{ lb-ft}$$

Table 2 707 flight test conditions

Flight test airplane	707-321B, N760PA
Initial pressure altitude	15,170 ft
Initial indicated airspeed	178 knots
Inital acceleration	-2.1 ft/s^2
Initial flight path angle	0.8 deg
Airplane gross weight	249,500 lb
Airplane center of gravity	34.5% MAC
Engine thrust	idle
Flaps/gear	up/up
Stabilizer setting	-4.0 deg FRL

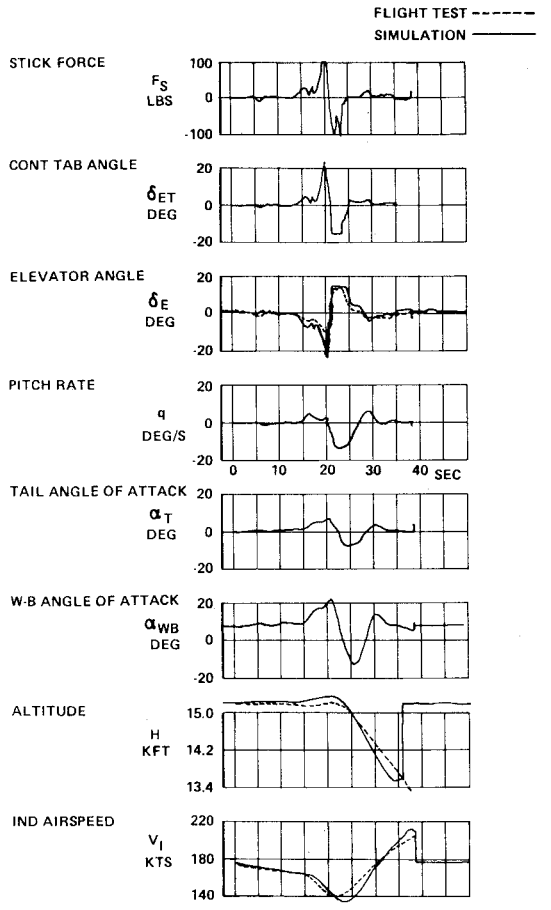

Fig. 10 Simulator time histories from combined wing-body-tail model.

Simulator Validation

A limited amount of simulator validation has been conducted to date. Much more data are required in order to examine the total flight envelope. However, these initial results are very encouraging. For substantiation of the math model formulated, a step-by-step verification was made at the subsystem level using existing ground test and flight test results.

An airplane static trim check was made by comparing the simulator's trim pitch attitude, stabilizer angle, and elevator angle to those from Boeing 707 flight test records.[10] The flight test data were matched for speed stability and elevator-stabilizer trade tests at both forward and aft c.g. cases. The airplane was trimmed at level flight. The comparison of results indicated that the separate wing-body and tail model offered a better static match compared to the conventional combined wing-body-tail model.

To provide a quantitative comparison of the dynamic response, a pullup and recovery longitudinal maneuver was selected from Boeing 707 certification flight test data.[11] The airplane flight conditions are tabulated in Table 2. The pilot stick force Fs from the flight test was input as a forcing function to the simulator. Simulator time histories of the elevator angle δ_E, pressure altitude H, and indicated airspeed V_I were compared with those from the flight test.

Figure 10 compares the time histories of the conventional combined wing-body-tail model with the flight test. A stabilizer angle of -3.5 deg, fuselage reference line (FRL), was used to obtain the initial match. The elevator response was oscillatory due to a single computer sampling time of 45 ms. Both altitude and airspeed responses show disparity relative to the flight test in magnitude and phase.

Shown in Fig. 11 are the corresponding time histories from the separate wing-body and tail model. Remarkably close

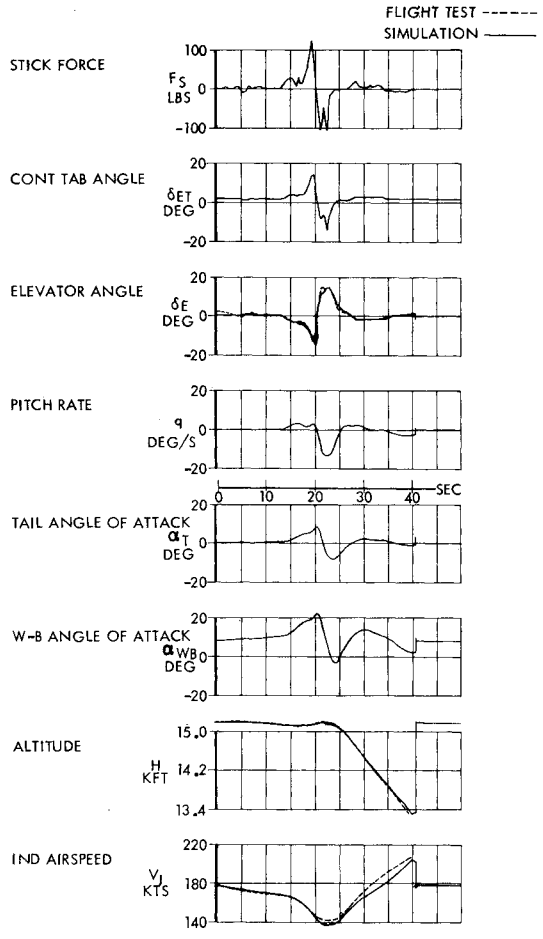

Fig. 11 Simulator time histories from separate wing-body and tail model.

correlations of control system and flight dynamics to actual flight test records have been achieved. No unusual correction factors were found necessary in order to establish this correlation for the case considered. Close examinations of the original computer strip chart revealed that the tail angle-of-attack time history leads in phase the wing-body by approximately 400 ms. A fixed base piloted simulation was conducted and the pilot commented that the separate wing-body and tail simulation model was very realistic.

Conclusions

A three-degree-of-freedom separate wing-body and tail simulation model has been developed for flight simulation. It offers the following potential improvements in comparison to the conventional combined wing-body-tail model:

1) Closer match to actual flight characteristics

2) More rigorous treatment of spatially related effects such as local unsteady aerodynamics, wing wake/downwash, wind and gust, ground effects and aeroelasticity properties

3) Better insight into basic design considerations by permitting independent assessment of parametric changes to the wing and tail

4) More efficient utilization of computational capacity

Extensive work remains to assess the potential improvements noted.

Appendix: Definition of Kinematic Angle of Attack

The following assumptions were made in deriving the kinematic angle of attack equation:

1) The Earth is assumed inertially fixed.

2) The airplane is considered rigid.

3) The airplane is assumed to have a longitudinal freedom only.

4) Wing wake/downwash, engine exhaust, ground effects, and wind/gust are totally neglected.

The aerodynamic angle of attack at a local point within the airplane can be defined by the equation:

$$\alpha_L \triangleq \tan^{-1} \frac{w_L}{u_L} \tag{A1}$$

where

u_L = X-direction component of the airplane body referenced translational velocity of a local point within the airplane

w_L = Z-direction component of the airplane body referenced translational velocity of a local point within the airplane

Differentiating Eq. (A1) with respect to time[12]

$$\dot{\alpha}_L = \frac{d\alpha_L}{dt} = \frac{u_L \dot{w}_L - \dot{u}_L w_L}{u_L{}^2 + w_L{}^2} \tag{A2}$$

where

$\dot{u}_L$ = X-direction component of the airplane body referenced translational acceleration of a local point within the airplane

$\dot{w}_L$ = Z-direction component of the airplane body referenced translational acceleration of a local point within the airplane

Now let us develop the equations for variables, $\dot{u}_L$, $\dot{w}_L$, u_L, and w_L. The position vector of a local point within the airplane can be expressed in the Earth axis system as x^e_L

$$x^e_L = x^e_0 + C^e_b x^b_{0L} \tag{A3}$$

where

x^e_0 = position vector of the airplane's center of gravity with respect to the fixed Earth reference point 0, coordinatized in the Earth axis system

x^b_{0L} = position vector of the local point with respect to the airplane's center of gravity, coordinatized in the airplane body axis system = $\{l_x, 0, l_z\}$

C^e_b = coordinate transformation matrix from the airplane body to Earth axis system

Differentiating both sides of Eq. (A3) with respect to time

$$\dot{x}^e_L = \dot{x}^e_0 + \dot{C}^e_b x^b_{0L} + C^e_b \dot{x}^b_{0L} \tag{A4}$$

We have the following relation[13]

$$\dot{C}^e_b = C^e_b \Omega^b_{eb} \tag{A5}$$

where Ω^b_{eb} is the skew-symmetric matrix of the airplane's body axis rotational velocity with respect to the Earth axis system, coordinatized in the body axis system.

We also assume that

$$x^b_{0L} = \text{constant} \tag{A6}$$

So that

$$\dot{x}^b_{0L} = 0 \tag{A7}$$

Substituting Eqs. (A5) and (A7) into Eq. (A4),

$$\dot{x}^e_L = \dot{x}^e_0 + C^e_b \Omega^b_{eb} x^b_{0L} \tag{A8}$$

Differentiating both sides of Eq. (A8) with respect to time

$$\ddot{x}_L^e = \ddot{x}_0^e + \dot{C}_b^e \Omega_{eb}^b x_{0L}^b + C_b^e \dot{\Omega}_{eb}^b x_{0L}^b + C_b^e \Omega_{eb}^b \dot{x}_{0L}^b \quad \text{(A9)}$$

Substituting Eqs. (A5) and (A7) into Eq. (A9),

$$\ddot{x}_L^e = \ddot{x}_0^e + C_b^e (\Omega_{eb}^b \Omega_{eb}^b + \dot{\Omega}_{eb}^b) x_{0L}^b \quad \text{(A10)}$$

where $\dot{\Omega}_{eb}^b$ is the skew-symmetric matrix of the airplane's body axis rotational acceleration with respect to the Earth axis system, coordinatized in the body axis system.

Premultiplying both sides of Eq. (A10) by C_e^b,

$$C_e^b \ddot{x}_L^e = C_e^b \ddot{x}_0^e + C_e^b C_b^e (\Omega_{eb}^b \Omega_{eb}^b + \dot{\Omega}_{eb}^b) x_{0L}^b \quad \text{(A11)}$$

where C_e^b is the coordinate transformation matrix from the Earth to airplane body axis system.

Since C_e^b is the inverse matrix of C_b^e and of nonsingular

$$C_e^b C_b^e = I \quad \text{(A12)}$$

where I is an indentity matrix.

Let A_L^b be defined as

$$A_L^b = C_e^b \ddot{x}_L^e \quad \text{(A13)}$$

where A_L^b is the inertially referenced linear acceleration of a local point within the airplane, coordinatized in the airplane body axis system.

Substituting Eqs. (A12) and (A13) into Eq. (A11),

$$A_L^b = C_e^b \ddot{x}_0^e + (\Omega_{eb}^b \Omega_{eb}^b + \dot{\Omega}_{eb}^b) x_{0L}^b \quad \text{(A14)}$$

An observer sitting at a local point and rotating with the airplane will see the translational acceleration of the local point in the following manner:[14]

$$\ddot{x}_L^b = A_L^b - \Omega_{eb}^b \dot{x}_L^b \quad \text{(A15)}$$

$\dot{x}_L^b$ in Eq. (A15) can be obtained by premultiplying Eq. (A8) by C_e^b and using Eq. (A12):

$$\dot{x}_L^b = C_e^b \dot{x}_L^e = C_e^b \dot{x}_0^e + \Omega_{eb}^b x_{0L}^b \quad \text{(A16)}$$

Substituting Eqs. (A14) and (A16) into Eq. (A15) and rearranging

$$\ddot{x}_L^b = C_e^b \ddot{x}_0^e - \Omega_{eb}^b C_e^b \dot{x}_0^e + \dot{\Omega}_{eb}^b x_{0L}^b \quad \text{(A17)}$$

The following relation is given[13]

$$C_e^b \dot{x}_0^e = \dot{x}_0^b + \Omega_{eb}^b x_0^b \quad \text{(A18)}$$

Conventionally, the origin of the earth axis system 0 is defined at the airplane's center of gravity,[1-3] then

$$x_0^b = 0 \quad \text{(A19)}$$

Hence, Eq. (A18) becomes

$$C_e^b \dot{x}_0^e = \dot{x}_0^b \quad \text{(A20)}$$

Substituting Eq. (A20) into Eq. (A17) yields

$$\ddot{x}_L^b = C_e^b \ddot{x}_0^e - \Omega_{eb}^b \dot{x}_0^b + \dot{\Omega}_{eb}^b x_{0L}^b \quad \text{(A21)}$$

Premultiplying both sides of Eq. (A20) by C_b^e and differentiating

$$\ddot{x}_0^e = \dot{C}_b^e \dot{x}_0^b + C_b^e \ddot{x}_0^b = C_b^e (\ddot{x}_0^b + \Omega_{eb}^b \dot{x}_0^b) \quad \text{(A22)}$$

Airplane body referenced translational acceleration vector at a local point can now be obtained by substituting Eq. (A22) into Eq. (A21):

$$\ddot{x}_L^b = \ddot{x}_0^b + \dot{\Omega}_{eb}^b x_{0L}^b \quad \text{(A23)}$$

where $\ddot{x}_0^b$ is the airplane body referenced translational acceleration vector of the airplane at the center of gravity $= \{\dot{u}, 0, \dot{w}\}$.

$\dot{x}_L^b$ can be obtained by integrating Eq. (A23)

$$\dot{x}_L^b = \int_0^t \ddot{x}_L^b \, dt + \dot{x}_{L0}^b \quad \text{(A24)}$$

where $\dot{x}_{L0}^b$ are the values of $\dot{x}_L^b$ at $t = 0$.

The matrix form of Eq. (A23) can be expressed as

$$\begin{bmatrix} \dot{u}_L \\ 0 \\ \dot{w}_L \end{bmatrix} = \begin{bmatrix} \dot{u} + l_z \dot{q} \\ 0 \\ \dot{w} - l_x \dot{q} \end{bmatrix} \quad \text{(A25)}$$

Integrating Eq. (A25)

$$\begin{bmatrix} u_L \\ 0 \\ w_L \end{bmatrix} = \begin{bmatrix} \int_0^t \dot{u}_L \, dt + u_{L0} \\ 0 \\ \int_0^t \dot{w}_L \, dt + w_{L0} \end{bmatrix} \quad \text{(A26)}$$

where u_{L0} is the value of u_L at $t = 0$, and w_{L0} is the value of w_L at $t = 0$.

By substituting values from Eqs. (A25) and (A26) into Eq. (A2), the local angle-of-attack rate $\dot{\alpha}_L$ can be calculated. The local angle of attack α_L can now be obtained by integrating $\dot{\alpha}_L$:

$$\alpha_L = \int_0^t \dot{\alpha}_L \, dt + \alpha_{L0} \quad \text{(A27)}$$

where α_{L0} is the value of α_L at $t = 0$.

Acknowledgment

This paper summarizes the work performed for the 707 product development program at the Boeing Commercial Airplane Company under supervision of F.C. Hall. I would like to thank M. Ivan and K.R. Britting for their valuable discussion and criticism on the definition of local angle of attack and dynamic derivatives. The EAI 8400 computer simulation was programmed by the Boeing Computer Services, Inc.

References

[1] Perkins, C.D. and Hage, R.E., *Airplane Performance, Stability and Control,* Wiley, New York, 1949.

[2] Etkin, B., *Dynamics of Atmospheric Flight,* Wiley, New York, 1972.

[3] McRuer, D., Ashkenas, I., and Graham, D., *Aircraft Dynamics and Automatic Control,* Princeton University Press, Princeton, N.J., 1973.

[4] Howe, R.M., "Coordinate Systems for Solving the Three-Dimensional Flight Equations," Wright Air Development Center TN 55-747, June, 1956.

[5] McFarland, R.E., "A Standard Kinematic Model for Flight Simulation at NASA Ames," Computer Science Corp., Mountain View, Calif., NASA CR-2497, Jan. 1975.

[6] Ayres, A.L., "Computing System Software Description and Operation for BCS-Renton Simulation Center," Boeing Document D183-10176, April 1972.

[7] Cameron, J.M., Modin, K.E., and Schweizer, W.L., "Improved Aerodynamic Data for the 707-300B (ADV)/C Flight Simulator," Boeing Document D6-24209, Nov. 1969.

[8] King, R.D., et al., "720B Full-Scale Horizontal Tail Wind Tunnel Test Result," unpublished Boeing Document, Nov. 1963.

[9] Roosme, A., et al.,, "707-320B(ADV)/C University of Washington Low Speed Wind Tunnel Test Result (UnWAL 1097)," unpublished Boeing Document, Aug. 1973.

[10] Modin, K.E. and Monroe, D.P., "Flight Simulator Aerodynamic Substantiation, 707-300B (ADV)/C," Boeing Document D6-24224, Feb. 1970.

[11] Stutsman, G.V., "Flight Test Summary Report, Commercial Transport Model 707-321B," Boeing Document D6-7157, May 1962.

[12] Selby, S.B., ed., *Standard Mathematical Tables,* 18th Ed., The Chemical Rubber Co., Cleveland, Ohio, 1970, p. 388.

[13] Britting, K.R., *Inertial Navigational Systems Analysis,* Wiley-Interscience, New York, 1971, pp. 17-18.

[14] Halfman, R.L., *Dynamics: Particles, Rigid Bodies and Systems,* Vol. I, Addison-Wesley, Reading, Mass., 1962, pp. 42-51.